

# Microscopic Route to Nematicity in $\text{Sr}_3\text{Ru}_2\text{O}_7$

Christoph M. Puetter,<sup>1</sup> Jeffrey G. Rau,<sup>1</sup> and Hae-Young Kee<sup>1,2,\*</sup>

<sup>1</sup>*Department of Physics, University of Toronto, Toronto, Ontario M5S 1A7 Canada*

<sup>2</sup>*School of Physics, Korea Institute for Advanced Study, Seoul 130-722, Republic of Korea*

An anisotropic metallic phase dubbed electronic nematic phase bounded by two consecutive metamagnetic transitions has been reported in the bilayer Ruthenate  $\text{Sr}_3\text{Ru}_2\text{O}_7$ . It has also been shown that the nematic and the accompanying metamagnetic transitions are driven by an effective momentum-dependent quadrupole-type interaction. Here, we study the microscopic origin of such an effective interaction. To elucidate the mechanism behind the spontaneous Fermi surface distortion associated with the nematic, we identify a simple tight binding model based on  $t_{2g}$  orbitals, spin-orbit coupling and the rotation of  $\text{RuO}_6$  octahedra as starting point, consistent with the Fermi surface obtained from recent angle resolved photoemission data. Within an extended Hubbard model the nematic state, characterized by an anisotropy between the bands near  $(\pm\pi, 0)$  and  $(0, \pm\pi)$ , then strongly competes with ferromagnetic order but preempts it via a finite nearest neighbour interaction. We discuss experimental means to confirm our proposal.

PACS numbers: 71.10.-w, 73.22.Gk

*Introduction* — In correlated electron systems, electrons can organize themselves in states that are analogous to classical liquid crystal phases [1]. The search for such phases in solid state systems, in particular for the quantum version of an anisotropic liquid crystal, dubbed electronic nematic phase, has been of great interest. Such a phase spontaneously breaks the point group symmetry of the underlying lattice thus characteristically modifying e.g. transport properties. Recently, a remarkable anisotropic longitudinal resistivity has been reported in the bilayer Ruthenate  $\text{Sr}_3\text{Ru}_2\text{O}_7$  [2], where the putative nematic phase is bounded by two consecutive metamagnetic transitions [3]. From a theoretical perspective, important progress has been made as well in understanding the phenomenon. It has been shown that an effective momentum-dependent interaction model [4–6] successfully describes the metamagnetic transitions occurring at the nematic phase boundaries [7], and the behaviour of the resistivity, when the magnetic field is applied along the  $c$ -axis [8] and tilted away from it [9].

However, the link between the effective interaction and the microscopic origin is missing. While attempts to illuminate the mechanism of nematic phase formation have been made very recently [10, 11], the focus exclusively lay on the quasi-1D Ru  $d_{yz}$  and  $d_{xz}$  orbitals, identifying the nematic phase as orbital ordering driven by an inter-orbital Hubbard interaction. Yet, there is no a priori reason to exclude the 2D  $d_{xy}$  orbital from the picture. On the contrary, angle resolved photoemission spectroscopy (ARPES) in the isotropic phase has revealed a van Hove singularity (vHS) near the Fermi level predominantly originating from the  $d_{xy}$  orbital [12]. This is crucial as the isotropic Fermi surface (FS) structure constrains the theoretical starting point for the study of the nematic phase within a weak coupling theory and the nematic is associated with a distortion of the FS topology [5, 6].

In this paper, we describe a microscopic route to ne-

maticity in  $\text{Sr}_3\text{Ru}_2\text{O}_7$ . We first model the underlying bandstructure including all three  $t_{2g}$  orbitals by incorporating unit cell doubling due to the rotation of the  $\text{RuO}_6$  octahedra and spin-orbit (SO) interaction into a single layer approach. We then show that the nematic phase is associated with a density imbalance in the  $\gamma_2$  band near  $(\pm\pi, 0)$  and  $(0, \pm\pi)$ , where the dominant orbital in the Bloch function is the  $d_{xy}$  orbital. We find that nematic ordering strongly competes with ferromagnetic order within a multi-orbital Hubbard model, but preempts it due to a finite nearest neighbor interaction. Ultimately, we discuss experimental probes to confirm our proposal.

*Fermi surface topology of  $\text{Sr}_3\text{Ru}_2\text{O}_7$*  — To obtain the electronic band structure we start from a single layer tight binding model with three  $t_{2g}$  orbitals and spin-orbit (SO) coupling, as in the case of the single layer Ruthenate  $\text{Sr}_2\text{RuO}_4$  [13, 14]. However, despite the similarity, two additional features need to be taken into account in the case of  $\text{Sr}_3\text{Ru}_2\text{O}_7$ : (1) a slight rotation of the RuO octahedra [15] entailing unit cell doubling, and (2) bilayer coupling. Here we proceed by including (1) and discuss the role of bilayer coupling later. The tight-binding band structure  $H_0$  then takes the form

$$H_0 = \sum_{\mathbf{k}} \Psi_{\mathbf{k}\uparrow}^\dagger \begin{pmatrix} A_{\mathbf{k}} & G \\ G^* & A_{\mathbf{k}+\mathbf{Q}} \end{pmatrix} \Psi_{\mathbf{k}\uparrow} + [\text{time reversed}],$$

$$A_{\mathbf{k}} = \begin{pmatrix} \varepsilon_{\mathbf{k}}^{yz} & \varepsilon_{\mathbf{k}}^{1D} + i\lambda & -\lambda \\ \varepsilon_{\mathbf{k}}^{1D} - i\lambda & \varepsilon_{\mathbf{k}}^{xz} & i\lambda \\ -\lambda & -i\lambda & \varepsilon_{\mathbf{k}}^{xy} \end{pmatrix}, \quad G = \bar{g}\mathbf{1}_{3\times 3} \quad (1)$$

where  $\Psi_{\mathbf{k}s}^\dagger = (\psi_{\mathbf{k}s}^{yz\dagger} \psi_{\mathbf{k}s}^{xz\dagger} \psi_{\mathbf{k}-s}^{xy\dagger} \psi_{\mathbf{k}+\mathbf{Q}s}^{yz\dagger} \psi_{\mathbf{k}+\mathbf{Q}s}^{xz\dagger} \psi_{\mathbf{k}+\mathbf{Q}-s}^{xy\dagger})$  consists of fermionic operators creating an electron with spin projection  $s = \uparrow, \downarrow$  in one of the three Ru  $t_{2g}$  derived orbitals  $\alpha = yz, xz, xy$ . The orbital dispersions are given by  $\varepsilon_{\mathbf{k}}^{xz} = -2t_1 \cos(k_x) - 2t_2 \cos(k_y)$ ,  $\varepsilon_{\mathbf{k}}^{yz} = -2t_1 \cos(k_y) - 2t_2 \cos(k_x)$ , and  $\varepsilon_{\mathbf{k}}^{xy} = -2t_3 (\cos(k_x) +$

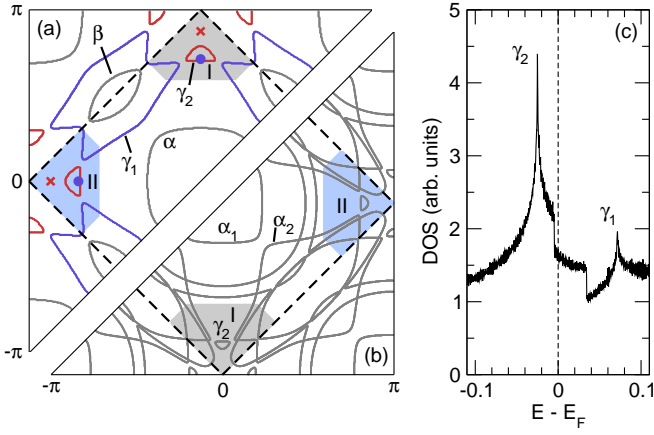


FIG. 1: (Color online) (a) Fermi surface of the single layer model. The crosses (dots) indicate the saddle points of the  $\gamma_2$  ( $\gamma_1$ ) band. The band structure parameters are  $t_1 = 0.5$ ,  $t_2 = 0.05$ ,  $t_3 = 0.5$ ,  $t_4 = 0.1$ ,  $t_5 = -0.03$ ,  $t_6 = 0.05$ ,  $\mu = 0.575$ ,  $\bar{g} = 0.1$ ,  $\lambda = 0.1375$ . (b) Fermi surface of the corresponding bilayer system with finite interlayer hopping between quasi-1D orbitals. (c) Total DOS near the Fermi level corresponding to (a). See main text for details.

$\cos(k_y)) - 4t_4\cos(k_x)\cos(k_y) - 2t_5(\cos(2k_x) + \cos(2k_y))$ , while  $\epsilon_{\mathbf{k}}^{1D} = -4t_6\sin(k_x)\sin(k_y)$  describes the hopping between the two quasi-1D orbitals and  $2\lambda\sum_i \mathbf{L}_i \mathbf{S}_i$  is the SO interaction [16] (all energies in the following are in units of  $2t_1$ ). For simplicity we have introduced unit cell doubling via an effective lattice potential  $\bar{g}$  with modulation vector  $\mathbf{Q} = (\pi, \pi)$ . The resulting Fermi surface and density of states (DOS) near the Fermi energy are shown in Fig. 1 (a) and (c), respectively, where all bands are doubly degenerate due to the lack of time reversal symmetry breaking.

As shown in Fig. 1 (a), the Fermi surface is composed of four sheets. The hole-like  $\alpha$  and electron-like  $\beta$  sheet are derived from quasi-1D orbitals, while the electron-like  $\gamma_1$  and hole-like  $\gamma_2$  sheet arise from quasi-1D and 2D orbital hybridization. The total DOS in Fig. 1 (c) reveals that the band structure provides two singularities near  $E_F$ , which originate from the  $\gamma_1$  and  $\gamma_2$  band. Since any instability in a weak coupling theory is boosted by a vHS near the Fermi level, these bands are most susceptible to a nematic transition. Consequently all other bands ( $\alpha$  and  $\beta$ ) can be rendered less important considering the nematic mechanism in  $\text{Sr}_3\text{Ru}_2\text{O}_7$ . For completeness we also show the effect of bilayer hopping in Fig. 1 (b). This FS, consistent with ARPES, exhibits a more complicated structure, where the  $\alpha_2$  sheet appears due to bilayer coupling (but not the  $\delta$  sheet, which most likely derives from  $e_g$  orbitals). However, since the orbital and topographical nature of the most singular  $\gamma$  bands near  $(\pm\pi, 0)$  and  $(0, \pm\pi)$  remains unaffected by a finite bilayer coupling, we proceed with the simpler single layer approach.

Indeed, not only are the  $\gamma$  bands responsible for the

vHS but the corresponding saddle points all lie within the shaded pocket regions I and II in Fig. 1 (a) (marked by crosses and dots). In region I (II), the  $\gamma_1$  and  $\gamma_2$  bands are mostly composed of only  $d_{yz}$  ( $d_{xz}$ ) and  $d_{xy}$  orbitals. For instance, the flat parts of the  $\gamma_2$  pockets and of the tips of the  $\gamma_1$  pockets derive from the quasi-1D orbital, while the curved portions and the  $\gamma_2$  saddle points have a strong  $d_{xy}$  character. Note that the  $\gamma_1$  and  $\gamma_2$  pockets are formed by hybridization via SO coupling, since even parity perturbations such as  $\bar{g}$  do not lift the degeneracy between quasi-1D and 2D orbitals due to different parity.

The simple orbital composition of the  $\gamma$  bands in regions I and II enables us to derive effective interactions within the  $\gamma$  bands involving only the highlighted pocket regions. The singularities in the DOS suggest that either one or both  $\gamma$  bands are involved in the formation of a nematic phase and that ordering can be driven by weak interactions due to a large DOS near the Fermi level. One should keep in mind, however, that there are more than one possible instabilities which take advantage of the vHS. Below, we study the interactions in the  $\gamma_2$  band in detail, and show how different orders compete.

*Microscopic route to nematicity* — The bilayer Ruthenate has a metallic ground state. Therefore, it is reasonable to assume that long-range interactions are well screened, leaving only moderately weak on-site and nearest neighbor interactions. The microscopic Hamiltonian then reads

$$H = H_0 + H_{\text{int}},$$

where the extended multi-orbital Hubbard interactions are given by

$$H_{\text{int}} = U \sum_{i,\alpha} n_{i\uparrow}^\alpha n_{i\downarrow}^\alpha + \tilde{U} \sum_{\substack{i,\alpha \neq \\ s,s'}} n_{is}^\alpha n_{is'}^\beta + \sum_{\substack{\langle i,j \rangle, \alpha \\ s,s'}} V^\alpha n_{is}^\alpha n_{js'}^\alpha \quad (2)$$

with  $n_{is}^\alpha = \psi_{is}^{\alpha\dagger} \psi_{is}^\alpha$  the density operator of the  $\alpha$  orbital on Ru site  $i$ . Here,  $U$ ,  $\tilde{U}$ , and  $V^\alpha$  represent repulsive on-site intra-orbital, on-site inter-orbital, and nearest neighbour intra-orbital interactions, respectively. To derive effective interactions, we write  $H_{\text{int}}$  in the basis of the Bloch bands, which can be accomplished straightforwardly as the  $\gamma$  bands in regions I and II are predominantly composed of two orbitals as discussed above. For region I, one thus obtains

$$\begin{pmatrix} a_{\mathbf{k}\sigma} \\ c_{\mathbf{k}\sigma} \end{pmatrix} = \begin{pmatrix} \cos\theta_{\mathbf{k}} & -\sin\theta_{\mathbf{k}} \\ \sin\theta_{\mathbf{k}} & \cos\theta_{\mathbf{k}} \end{pmatrix} \begin{pmatrix} \psi_{\mathbf{k}+\mathbf{Q}s}^{xy} \\ \psi_{\mathbf{k}-s}^{yz} \end{pmatrix}, \quad (3)$$

where  $a_{\mathbf{k}\sigma}$  and  $c_{\mathbf{k}\sigma}$  represent the annihilation of a quasiparticle with momentum  $\mathbf{k}$  and pseudospin  $\sigma = \pm$  in the  $\gamma_1$  and  $\gamma_2$  band, respectively. The mixing angles are given by  $\{\sin\theta_{\mathbf{k}}, \cos\theta_{\mathbf{k}}\} = 0.5 \left[ 1 \pm (\epsilon_{\mathbf{k}+\mathbf{Q}}^{xy} - \epsilon_{\mathbf{k}}^{yz}) / \sqrt{(\epsilon_{\mathbf{k}+\mathbf{Q}}^{xy} - \epsilon_{\mathbf{k}}^{yz})^2 + |\Gamma_{\mathbf{k}}^{xy,yz}|^2} \right]^{1/2}$ , where  $\Gamma_{\mathbf{k}}^{xy,yz}$  denotes the effective orbital hybridization mainly caused

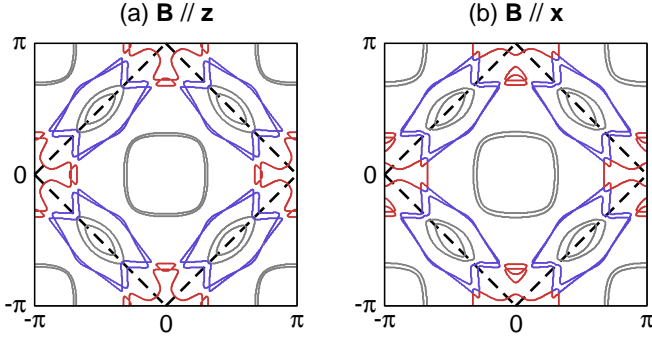


FIG. 2: (Color online) Effect of an external magnetic field on the band structure for field orientations (a) parallel to the  $z$  axis and (b) parallel to the  $x$  axis with  $B = 0.05$ .

by SO interaction. Likewise, the  $\gamma$  bands can be approximated in region II by substituting the  $d_{yz}$  for the  $d_{xz}$  orbital (or, equivalently, by exchanging  $k_x \leftrightarrow k_y$ ).

Focusing on the  $\gamma_2$  band, the effective interaction then has the form

$$\sum_{\substack{\mathbf{k}_1, \mathbf{k}_2 \in \text{I} \\ \text{or } \in \text{II}}} U_1 n_{\mathbf{k}_1 + \mathbf{k}_2} + \sum_{\substack{\mathbf{k}_1 \in \text{I} \\ \mathbf{k}_2 \in \text{II}}} [U_2 n_{\mathbf{k}_1 \sigma} n_{\mathbf{k}_2 \sigma} + U_3 n_{\mathbf{k}_1 \sigma} n_{\mathbf{k}_2 - \sigma}],$$

where  $n_{\mathbf{k}\sigma} = c_{\mathbf{k}\sigma}^\dagger c_{\mathbf{k}\sigma}$  and the interaction strengths are

$$\begin{aligned} U_1 &= U(\sin^2\theta_{\mathbf{k}_1}\sin^2\theta_{\mathbf{k}_2} + \cos^2\theta_{\mathbf{k}_1}\cos^2\theta_{\mathbf{k}_2}) \\ &\quad + 2\tilde{U}\sin^2\theta_{\mathbf{k}_1}\cos^2\theta_{\mathbf{k}_2} + 4V\sin^2\theta_{\mathbf{k}_1}\sin^2\theta_{\mathbf{k}_2}, \\ U_2 &= \tilde{U}(\sin^2\theta_{\mathbf{k}_1}\cos^2\theta_{\mathbf{k}_2} + \cos^2\theta_{\mathbf{k}_1}\sin^2\theta_{\mathbf{k}_2}) \\ &\quad + \tilde{U}\cos^2\theta_{\mathbf{k}_1}\cos^2\theta_{\mathbf{k}_2} + 8V\sin^2\theta_{\mathbf{k}_1}\sin^2\theta_{\mathbf{k}_2}, \\ U_3 &= U\sin^2\theta_{\mathbf{k}_1}\sin^2\theta_{\mathbf{k}_2} + \tilde{U}(2\sin^2\theta_{\mathbf{k}_1}\cos^2\theta_{\mathbf{k}_2} \\ &\quad + \cos^2\theta_{\mathbf{k}_1}\cos^2\theta_{\mathbf{k}_2}) + 4V\sin^2\theta_{\mathbf{k}_1}\sin^2\theta_{\mathbf{k}_2}, \end{aligned} \quad (4)$$

Here, we have included only the largest nearest neighbor contribution  $V^{xy} = V$ .

Obviously, different instabilities compete. The dominant one is determined by the mixing parameters and the bare interaction strengths. To investigate the qualitative features of the model we take advantage of the small size of regions I and II and approximate the form factors by their averages  $s^2 = \langle \sin^2\theta_{\mathbf{k}} \rangle = 0.656$  and  $c^2 = \langle \cos^2\theta_{\mathbf{k}} \rangle = 0.344$ , which signifies the dominance of the  $d_{xy}$  orbital [17].  $H_{\text{int}}$  then can be decoupled naturally into a nematic (n), a nematic spin-nematic (nsn), and a magnetic (M) channel [18]:

$$\begin{aligned} \Delta_n &= \sum_{\sigma} (n_{\sigma}^{\text{I}} - n_{\sigma}^{\text{II}}), \\ \Delta_{\text{nsn}} &= \sum_{\sigma} \sigma (n_{\sigma}^{\text{I}} - n_{\sigma}^{\text{II}}), \\ \Delta_{\text{M}} &= \sum_{\sigma} \sigma (n_{\sigma}^{\text{I}} + n_{\sigma}^{\text{II}}), \end{aligned} \quad (5)$$

with  $n_{\sigma}^{\text{I/II}} = N^{-1} \sum_{\mathbf{k} \in \text{I/II}} n_{\mathbf{k}\sigma}$  and  $N$  the number of  $\mathbf{k}$  points within each region. All in all, one thus arrives at

the following mean field Hamiltonian for the  $\gamma_2$  band

$$\begin{aligned} H^{\text{MF}} &= \frac{1}{N} \sum_{\substack{\mathbf{k} \in \text{I, II} \\ \sigma = \pm}} (E_{\mathbf{k}\sigma} - V_n \Delta_n \rho_{\mathbf{k}} - V_{\text{nsn}} \Delta_{\text{nsn}} \sigma \rho_{\mathbf{k}}) \\ &\quad - V_{\text{M}} \Delta_{\text{M}} \sigma) c_{\mathbf{k}\sigma}^\dagger c_{\mathbf{k}\sigma} + V_n \Delta_n^2 + V_{\text{M}} \Delta_{\text{M}}^2 + V_{\text{nsn}} \Delta_{\text{nsn}}^2, \end{aligned} \quad (6)$$

where  $E_{\mathbf{k}\sigma}$  denotes the  $\gamma_2$  quasiparticle bands and  $\rho_{\mathbf{k}}$  is set to  $+(-)$  for  $\mathbf{k} \in \text{I} (\text{II})$ . The effective interaction parameters are given by

$$\begin{aligned} V_n &= (-0.5U + \tilde{U})c^4 + \tilde{U}s^2c^2 + 4Vs^4, \\ V_{\text{nsn}} &= 0.5Uc^4 + \tilde{U}s^2c^2 + 4Vs^4, \\ V_{\text{M}} &= 0.5Uc^4 + \tilde{U}s^2c^2 + Us^4. \end{aligned} \quad (7)$$

Note that  $V$  affects only the nematic channels. While the above analysis is carried out for the  $\gamma_2$  band, it is also valid for the tips of the  $\gamma_1$  band inside regions I and II with similar effective interaction strengths.

*Effect of magnetic field and phase diagram* — The anomalous behaviour of the bilayer Ruthenate is exposed in the presence of an external magnetic field, which can be included straightforwardly via Zeeman coupling  $H_{\text{B}} = -\mathbf{B} \sum_i (\mathbf{L}_i + 2\mathbf{S}_i)$ . A field along the  $z$  axis, however, only renormalizes the spin dependent chemical potential due to a quenching of orbital moments. The FS therefore changes according to the dominant underlying spin character at each  $\mathbf{k}$  point (see Fig. 2 (a)). Tilting the magnetic field towards the  $x$  axis introduces anisotropy into the system via SO coupling (Fig 2 (b)). It also increases the mixing of the  $t_{2g}$  orbitals in the pocket regions, where the  $\gamma_2$  FS sheet undergoes a pronounced topological change and the tips of the  $\gamma_1$  sheet are distinctly distorted. A tilted field therefore implicates a low (high) longitudinal conductivity parallel (perpendicular) to the in-plane field component (not shown), in agreement with the experimental findings in the nematic phase [2].

In Fig. 3 we show the mean field phase diagram as a function of magnetic field along the  $z$  axis and  $V$  for  $U = 0.17$ ,  $\tilde{U} = 0.76U$ , and the band structure parameters specified in Fig. 1. Since the rotation angles and the size of the  $\text{RuO}_6$  octahedra vary throughout the Ruthenate family [15, 19–21], the nearest neighbour interaction  $V$  is the most eminent interaction parameter in the present model. As expected from Eq. (7),  $V$  promotes nematicity with increasing magnitude. On the other hand, as  $V$  decreases, the nematic window shrinks and the phase boundaries, which are of first order and coincide with metamagnetic jumps [7], merge into a single line of metamagnetic transitions. Driving the magnetic field strength up at small  $V/U$ , e.g. along the blue dashed line, tunes one of the  $\gamma_2$  vHS close enough to the Fermi level to induce a nematic transition. This transition may also involve additional bands (like  $\gamma_1$ ) due to effective interband interactions. Note that the effect of

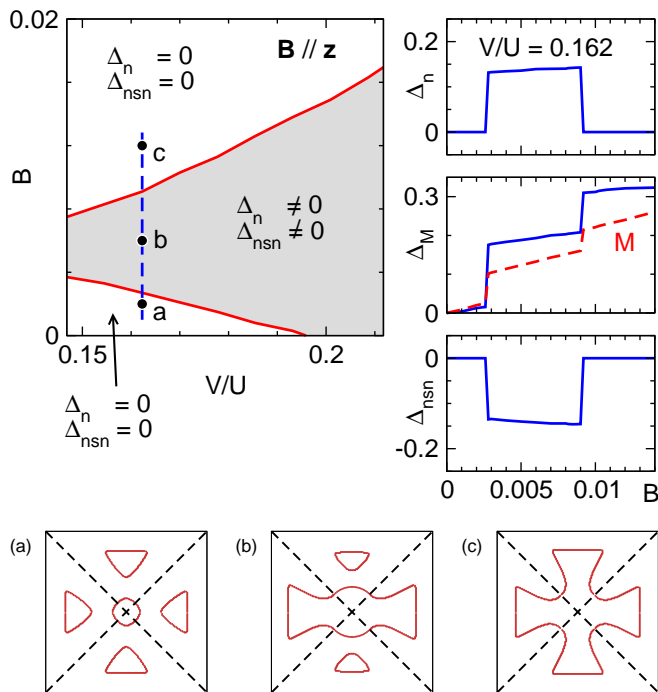


FIG. 3: (Color online) Mean field phase diagram. The order parameters exhibit dramatic jumps, and the magnetization  $M$  is shown as a red dashed line in the  $\Delta_M$  panel. Panels (a) - (c) display the FS evolution of the nematic  $\gamma_2$  band near  $(\pm\pi, 0)/(0, \pm\pi)$  along the blue dashed line. See main text for details.

bilayer hopping in the presence of an in-plane field has been studied previously [9] but is expected to have only a minor influence on nematic ordering. Note also, that in the present context nematic order characterizes the difference in the electronic or quasiparticle density near  $(\pm\pi, 0)$  and  $(0, \pm\pi)$ . The phenomenological order parameter  $\sum_{\mathbf{k}}(\cos(k_x) - \cos(k_y))n_{\mathbf{k}}$  used in previous studies [5–9] therefore captures the nematic phase remarkably well.

*Discussion and summary* — We have described a microscopic mechanism for nematicity in the bilayer Ruthenates. Our proposal is based on a simple tight binding approach including all three  $t_{2g}$  orbitals, SO interaction, and unit cell doubling. Leaving interactions aside, this approach leads to a realistic band structure with a FS similar to recent ARPES data. Including interactions, the most sensitive band is predominantly composed of folded  $d_{xy}$  and unfolded quasi-1D orbitals near  $(\pm\pi, 0)$  and  $(0, \pm\pi)$ , where it undergoes pronounced anisotropic changes in the nematic phase. We find that the on-site intra-orbital interaction strongly favors ferromagnetic order over any nematic order. On-site inter-orbital interaction on the other hand slightly favors nematic order over both ferromagnetic and nematic spin-nematic channels leading to a rather non-trivial and strong competition between all channels. However, the

nearest neighbour interaction drastically enhances charge and spin-nematic susceptibilities, sufficient to induce a nematic transition in at least one of the FS components by applying a moderate magnetic field, and thus preempting ferromagnetic order.

Our results imply that nematic order is sensitive to the location of vHS and the balance between competing instabilities. The combination of SO coupling and rotation of  $\text{RuO}_6$  octahedra plays a crucial role in generating flat bands and the vHS near the corners of the reduced Brillouin zone  $(\pm\pi, 0)$  and  $(0, \pm\pi)$ , where the band structure is most susceptible to change. Among the members of the Ruthenate family,  $\text{Ca}_{1.8}\text{Sr}_{0.2}\text{RuO}_4$  shows a similar metamagnetic transition [23] and neutron scattering pattern [24] as non-ultra-clean  $\text{Sr}_3\text{Ru}_2\text{O}_7$  [25, 26]. The  $\text{RuO}_6$  octahedra are also rotated, which distinguishes this compound from pure  $\text{Sr}_2\text{RuO}_4$ , in addition to the introduction of disorder. Therefore, it is tempting to argue that there also exists a hidden (due to disorder) nematic phase as in the case of non-ultra-clean  $\text{Sr}_3\text{Ru}_2\text{O}_7$ .

Furthermore, a recent experiment probing the entropy landscape [22] has indicated critical behavior outside the nematic window. It is possible that criticality arises from an uncovered critical point (or weak first order transition) outside, yet nearby, the nematic phase space. An earlier work [6] has shown that the nematic window shrinks as interactions decrease, and in fact becomes exponentially small where critical fluctuations become important. However, origin and nature of critical fluctuations outside the nematic are beyond the scope of the current mean field study.

It is worthwhile to comment on the difference between our proposal and the one in Ref. [10, 11], where nematic order is associated with orbital ordering between the two quasi-1D orbitals, and the anisotropy appears in the  $\alpha_1$  and  $\alpha_2$  FS sheets near the  $\Gamma$  point. A possible way to distinguish both proposals is scanning tunneling microscopy [27], which in principle should probe all bands. Quantum oscillations would be another way [28], since the  $\gamma_2$  frequency should drastically change between the two isotropic phases indicated in Fig. 3 (a) and (c), and, although difficult to observe, should split into two when passing through the nematic phase.

*Note added* — After we posted the manuscript on the arXiv, we were informed of a related study by M. H. Fischer and M. Sigrist [29].

We thank Y. Sidis, R. S. Perry, A. P. Mackenzie, A. Green, H. Tagaki, S. Kivelson, Y. J. Kim, and especially A. Paramekanti for useful discussions. HYK acknowledges the University of Tokyo for their hospitality. This work was supported by NSERC of Canada, Canada Research Chair, and Canadian Institute for Advanced Research.

- 
- \* Electronic address: hykee@physics.utoronto.ca
- [1] S. A. Kivelson *et al.*, Nature **393**, 550 (1998).
- [2] R. A. Borzi *et al.*, Science **315**, 214 (2007).
- [3] S. A. Grigera *et al.*, Science **306**, 1154 (2004).
- [4] V. Oganesyan *et al.*, Phys. Rev. B **64**, 195109 (2001).
- [5] H.-Y. Kee *et al.*, Phys. Rev. B **68**, 245109 (2003).
- [6] I. Khavkine *et al.*, Phys. Rev. B **70**, 184521 (2004).
- [7] H.-Y. Kee and Y. B. Kim, Phys. Rev. B **71**, 184402 (2005).
- [8] H. Doh *et al.*, Phys. Rev. Lett. **98**, 126407 (2007).
- [9] C. Puetter *et al.*, Phys. Rev. B **76**, 235112 (2007).
- [10] S. Raghu *et al.*, Phys. Rev. B **79**, 214402 (2009).
- [11] W.-C. Lee and C. Wu, Phys. Rev. B **80**, 104438 (2009).
- [12] A. Tamai *et al.*, Phys. Rev. Lett. **101**, 026407 (2008).
- [13] C. Bergemann *et al.*, Phys. Rev. Lett. **84**, 2662 (2000).
- [14] K. M. Shen *et al.*, Phys. Rev. B. **64**, 180502(R) (2001).
- [15] H. Shaked *et al.*, J. Solid State Chem. **154**, 361 (2000).
- [16] K. K. Ng and M. Sigrist, Europhys. Lett. **49**, 473 (2000).
- [17] The actual values of the mixing parameters near the  $\gamma_2$  saddle points are larger due to a stronger  $d_{xy}$  admixture (thus effectively enhancing  $V_n$  and  $V_{nsn}$ ). However, this only changes quantitative details such as the location of the phase boundary in Fig. 3.
- [18] Considering the FS structure another competing order is a spin density wave (SDW) state, which breaks the translational and spin-rotational symmetry. However, it was explicitly shown in Ref. [10] that SDW order is suppressed by SO coupling. This is consistent with our intuition as the spin is no longer a good quantum number in the presence of SO coupling.
- [19] M. N. Iliev *et al.*, Physica B **358**, 138 (2005).
- [20] K. Iwata *et al.*, J. Phys. Soc. Jpn. **77**, 104716 (2008).
- [21] Y. Yoshida *et al.*, Phys. Rev. B **72**, 054412 (2005).
- [22] A. W. Rost *et al.*, Science **325**, 1360 (2009).
- [23] J. Baier *et al.*, J. Low Temp. Phys. **147**, 405 (2007).
- [24] P. Steffens *et al.*, Phys. Rev. Lett. **99**, 217402 (2007).
- [25] R. S. Perry *et al.*, Phys. Rev. Lett. **86**, 2661 (2001).
- [26] L. Capogna *et al.*, Phys. Rev. B **67**, 012504 (2003).
- [27] H. Doh and H. Y. Kee, Phys. Rev. B. **75**, 233102 (2007).
- [28] J. F. Mercure *et al.*, arXiv:0909.1215v1.
- [29] M. H. Fischer and M. Sigrist, arXiv:0909.5392v1.